Intermediate scattering potential strength in electron-irradiated YBa$_2$Cu$_3$O$_{7-\delta}$ from London penetration depth measurements

Kyuil Cho [1,2] M. Kończykowski [3] S. Teknowijoyo [1,2] S. Ghimire [1,2] M. A. Tanatar [1,2]
Vivek Mishra [4] and R. Prozorov [1,2,*]

[1]*Ames Laboratory, Ames, IA 50011, USA*
[2]*Department of Physics & Astronomy, Iowa State University, Ames, IA 50011, USA*
[3]*Laboratoire des Solides Irradiés, École Polytechnique, CNRS, CEA, Institut Polytechnique de Paris, F-91128 Palaiseau, France*
[4]*Kavli Institute for Theoretical Sciences, University of Chinese Academy of Sciences, Beijing 100190, China*

Temperature-dependent London penetration depth, $\lambda(T)$, of a high quality optimally doped YBa$_2$Cu$_3$O$_{7-\delta}$ single crystal was measured using a tunnel-diode resonator. Controlled artificial disorder was induced at a low temperature of 20 K by 2.5 MeV electron irradiation with the accumulation of large doses of 3.8×10^{19} and 5.3×10^{19} electrons per cm^2. The irradiation caused significant suppression of the superconductor's critical temperature, T_c, from 94.6 to 90.0 K and then to 78.7 K, respectively. The low-temperature behavior of $\lambda(T)$ evolves from a T linear in pristine state to a T^2 behavior after the irradiation, expected for a line-nodal d-wave superconductor. However, the original theory that explained such behavior had assumed a unitary limit of the scattering potential, whereas usually in normal metals and semiconductors, Born scattering is sufficient to describe the experiment. To estimate the scattering potential strength, we calculated the normalized superfluid density, $\rho_s(t = T/T_c) = \lambda^2(0)/\lambda^2(t)$, varying the amount and the strength of nonmagnetic scattering using a self-consistent t-matrix theory. Fitting the obtained curves to a power law, $\rho_s = 1 - Rt^n$, and to a polynomial, $\rho_s = 1 - At - Bt^2$, and comparing the coefficients n in one set and A and B in another with the experimental values, we estimate the phase shift to be around 70 and 65°, respectively. We correlate this result with the evolution of the density of states with nonmagnetic disorder.

I. INTRODUCTION

While the microscopic mechanism of superconductivity is still actively debated three decades after its discovery [1], it is universally accepted that at least optimally doped high T_c cuprates have nodal, d-wave symmetry of the order parameter [2–6]. Line nodes in the gap function result in linear in energy density of states which lead to a T-linear variation of the superfluid density at low temperatures, where "low," roughly $T_c/3$, is defined as the temperature below which the superconducting order parameter amplitude is nearly constant; thus the density of nodal quasiparticles is determined solely by the angular variation of the superconducting gap on the Fermi surface. Indeed, measured linear temperature dependence of $\lambda(T)$ was among the first definitive arguments in favor of a d-wave superconductivity in YBa$_2$Cu$_3$O$_{7-\delta}$ (YBCO) [7,8].

Another consequence of anisotropic (and, in extreme cases, nodal) order parameter is the violation of the Anderson theorem [9], satisfied only for isotropic gap and nonmagnetic scatterers. Abrikosov and Gor'kov showed that spin-flip scattering from magnetic impurities suppresses even isotropic superconducting gap [10]. In the case of anisotropic superconducting gap, the order parameter (hence T_c) is suppressed by both magnetic and nonmagnetic impurities [11–14] and this can be readily extended to multiband superconductors [15,16].

This universal suppression of T_c by all types of disorder was indeed observed in YBCO [17–19].

As far as low-temperature variation of $\Delta\lambda(T)$ is concerned, already early experiments showed a crossover from T linear to a T^2 variation of $\lambda(T)$, for example in Zn-doped YBa$_2$Cu$_3$O$_{6.95}$ [20,21]. These results were explained by Hirschfeld and Goldenfeld [11], but in order to provide a quantitative agreement with the experiment they had to postulate unitary limit of the impurity scattering. Since usually the opposite, weak scattering (Born) limit explains the properties of normal metals, this feature of their theory was puzzling and attracted significant experimental and theoretical follow-up [22]. Analysis of the optical spectroscopy data led to a conclusion that the intermediate (between Born and unitary) scattering phase shifts describe YBCO [8]. We note that the majority of works studying disorder in superconductors focuses on the suppression of T_c and there is little known about low-temperature thermodynamics. During the past decade we studied both the variation of T_c and the changes in $\lambda(T)$, focusing on iron-based superconductors [23,24] and here we conduct a similar study of YBa$_2$Cu$_3$O$_{7-\delta}$.

Experimentally, it is not trivial to introduce a nonmagnetic point-like disorder. Chemical substitution perturbs the stoichiometry and may change the electronic band structure. One of the clean ways to do this is to use particle irradiation, which was used for metals extensively since the middle of the past century [25,26]. Among all projectiles, relativistic electrons provide just enough energy to induce vacancy-interstitial Frenkel pairs. If the irradiation is

*Corresponding author: prozorov@ameslab.gov

conducted at low temperatures, the recombination and clustering are inhibited and on warming, the interstitials migrate to various sinks (dislocations, twin boundaries, surfaces) leaving behind a quasiequilibrium population of vacancies that act as point-like scattering centers. A good check of the metastable nature is the (sometimes complete) recovery of properties on annealing signaling that the irradiation did not cause an irreversible damage. More details on using electron irradiation for superconductors can be found elsewhere [24]. In YBCO, the effect of electron irradiation on transport properties and transition temperature is described in Refs. [17–19].

We used relatively large doses of electron irradiation to induce nonmagnetic point-like disorder in a high quality optimally doped YBa$_2$Cu$_3$O$_{7-\delta}$ single crystal. The measured suppression of the superconducting transition temperature, T_c, gives the estimate of the dimensionless scattering rate Γ/T_{c0} (see Appendix), whereas the variation of the low-temperature London penetration depth, $\Delta\lambda(t)$, is related directly to the normalized superfluid density, $\rho_s(t) \approx 1 - 2\Delta\lambda(t)/\lambda(0)$, whose temperature dependence is sensitive to the structure of the superconducting order parameter [23,27]. Here $t = T/T_c$ is the (scattering-dependent) reduced temperature, and $\lambda(0)$ is the magnitude of the London penetration depth at $T = 0$. The impurity potential is parameterized in terms of the scattering phase shift, where very small values correspond to weak scattering centers (Born limit) and a phase shift close to $\theta = 90°$ represents unitary scatterers. (Note that in the figures we show $\theta \to 0°$ for Born limit for convenience. Of course, there is a small phase shift even in that regime.) We used t-matrix theory to calculate the superfluid density and then fitted the experimental and numerical data to the same models. This leads to the estimates the phase shift in YBCO at $\theta = 65 - 70°$, which agrees with the theoretical conclusion that the phase shift is intermediate between Born and unitary limits [8]. These values correspond to a regime where the density of states close to zero energy become sensitive to scattering.

II. EXPERIMENTAL

Single crystals YBa$_2$Cu$_3$O$_{7-\delta}$ were grown in yttria stabilized zirconia crucibles with subsequent annealing to achieve the highest transition temperature as described elsewhere [28]. Similar crystals were used in multiple studies with the variety of techniques. The crystal used for the current study has dimensions of $0.8 \times 0.51 \times 0.01$ mm^3.

The 2.5 MeV electron irradiation was performed at the SIRIUS Pelletron facility of the Laboratoire des Solides Irradiés (LSI) at the École Polytechnique in Palaiseau, France [18,24]. The acquired irradiation dose is conveniently measured in C/cm^2, where 1 C/cm$^2 = 6.24 \times 10^{18}$ electrons/cm^2. The same crystal was irradiated twice, first receiving a dose of 6.15 C/cm^2 (3.8×10^{19} electrons per cm^2) after which the measurements were repeated, and then more irradiation was added bringing the total cumulative dose of 8.5 C/cm^2 (5.3×10^{19} electrons per cm^2). Appendix B details the irradiation cross-sections and provides more information on the damage induced.

The in-plane London penetration depth $\Delta\lambda$ (T) was measured before and after each irradiation run using a self-oscillating tunnel-diode resonator technique (TDR) described

in detail elsewhere [23,27,29–32]. The TDR circuit resonates at $\sim$14 MHz and the frequency shift is measured with precision better than one part per billion. The inductor coil generates an AC excitation magnetic field, $H_{ac} < 20$ mOe; hence the sample is always in the Meissner state at the temperatures of interest. In the experiment, the sample was mounted on a 1 mm-diameter sapphire rod and inserted into a 2 mm-diameter inductor coil. The coil and the sample are in vacuum inside a ^{3}He cryostat. The TDR circuit is actively stabilized at 5 K, and the sample temperature is controlled separately from 0.4 K up by independent LakeShore controllers. It is straightforward to show that the change of the resonant frequency when a sample is inserted into the coil is proportional to the sample magnetic susceptibility as long as the change of the total inductance is small and one can expand, $\Delta f/f_0 \approx -\Delta L/2L_0$, where $2\pi f_0 = 1/\sqrt{CL_0}$ with subscript "0" referring to an empty resonator. The coefficient of proportionality that includes the demagnetization correction is measured directly by pulling the sample out of the resonator at the base temperature [30,33].

In this work we analyze the variation of the London penetration depth, $\Delta\lambda = \lambda(T) - \lambda(T_{\min}) \approx \lambda(T) - \lambda(0)$, where $T_{\min} = 0.02T_c$ is the minimum temperature of the experiment. The normalized superfluid density $\rho_s \equiv \lambda^2(0)/\lambda^2(T) = 1/(1 + \Delta\lambda/\lambda(0))^2 \approx 1 - 2\Delta\lambda/\lambda(0)$. This ratio does not depend on $\lambda(0)$ because the penetration depth is given roughly by $\lambda(t)/\lambda(0) \approx 1/\sqrt{1 - t^p}$ in the whole temperature interval, $0 \leqslant t \leqslant 1$ [27]. Here $t = T/T_c$ and the exponent $p = 2$ or 4 depending on the pairing type [27]. Therefore measurements of $\Delta\lambda(t)$ provide direct access to the structure of the superconducting order parameter via the superfluid density, $\rho_s(t)$.

III. RESULTS AND DISCUSSION

Figure 1 shows the variation of London penetration depth in the same crystal measured before and after two exposures to 2.5 MeV electron irradiation. As shown in the inset, the pristine sample exhibits a sharp transition at 94.6 K, indicative of a high quality optimally doped crystal [6]. On irradiation, T_c (onset) substantially decreased, first from 94.6 K in the pristine state to 90.0 K after 6.15 C/cm^2 and then to 78.7 K after a total dose of 8.5 C/cm^2 was applied. The sharp superconducting transition in the pristine sample, $\Delta T_c < 0.8$ K, becomes broader after the first irradiation run, $\Delta T_c = 6.5$ K at 6.15 C/cm^2, but then becomes narrower, $\Delta T_c = 5.1$ K, after 8.5 C/cm^2. The broadening is most likely due to some initial inhomogeneity of the produced defects density, which becomes more homogeneous in time upon slow natural annealing at room temperature. The measurement after first irradiation of 6.15 C/cm^2 was conducted rather quickly within a week of the irradiation run, but the measurement after second irradiation bringing the total dose to 8.5 C/cm^2 was made about a month later. Perhaps this will be interesting to study separately, but for the present work it is important that the transition temperature is well defined and that the region of the broader transition is far from the low-temperature region of interest for the fitting of the London penetration depth.

There are two ways to analyze the differences between the curves presented in Fig. 1. One is to perform a power-law fitting up to 0.3 T_c, $\Delta\lambda \sim T^n$, which has been extensively used
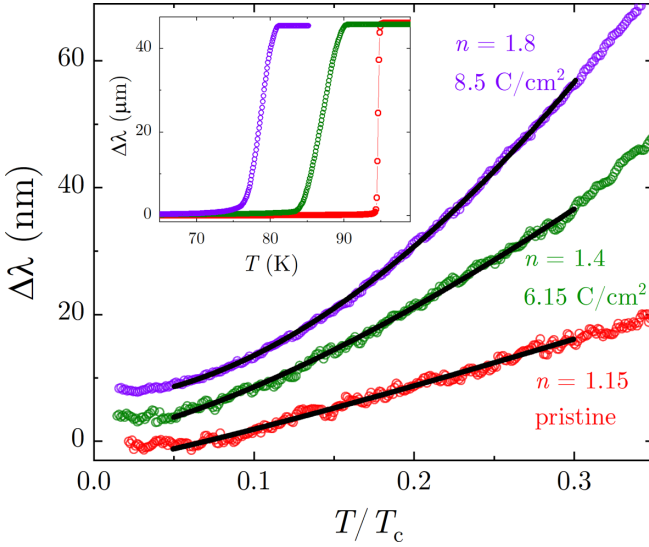
FIG. 1. Variation of the London penetration depth, $\Delta\lambda(t)$, measured before and after the 2.5 MeV electron irradiation first with a dose of 6.15 C/cm^2 (3.8×10^{19} electrons per cm^2), and then more irradiation was added bringing the total cumulative dose of 8.5 C/cm^2 (5.3×10^{19} electrons per cm^2). The main panel shows $\Delta\lambda(t)$ vs $t = T/T_c$ fitted to the power law, $\Delta\lambda(t) \propto t^n$. The exponent n changes from practically linear, $n = 1.15$ in the pristine sample to $n = 1.8$ on irradiation, suggesting the crossover from t linear to t^2 dependence. The inset shows a full temperature range showing the substantial suppression of T_c by the irradiation.
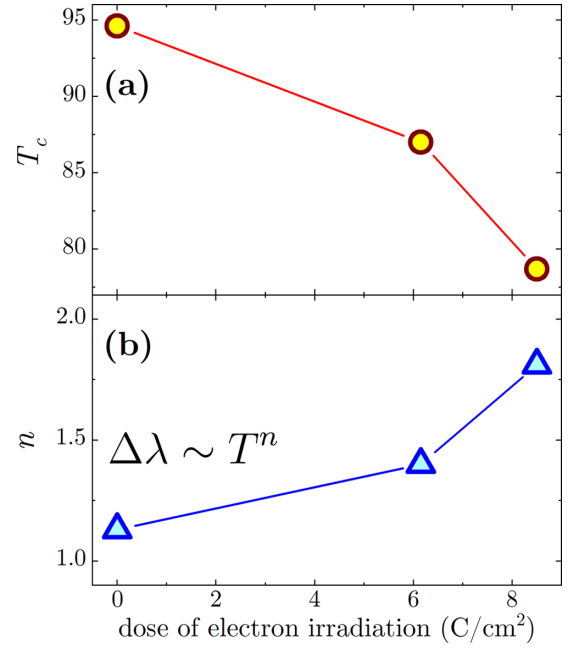

FIG. 2. Analysis of the data presented in Fig. 1. (a) Superconducting transition temperature, T_c. (b) Power-law exponent, n, as a function of the cumulative dose of electron irradiation showing a systematic evolution from a clean T linear to a dirty T^2 behavior expected for a d-wave superconductor.

for the analysis of pair-breaking scattering in $s_\pm$ iron-based superconductors [23,24]. Another is to perform a polynomial fit, $2\Delta\lambda/\lambda(0) = At + Bt^2$, where the factor of 2 comes from the expansion, $\rho_s \approx 1 - 2\Delta\lambda/\lambda(0)$. The former approach has an advantage of being independent of $\lambda(0)$, because only the exponent n matters. However, using exponent n as a fitting parameter is more sensitive to the choice of the fitting range and it has a less transparent meaning for dimensional quantities. The quadratic polynomial is a standard way to analyze such results and it offers both coefficients A and B which, however, depend on the choice of $\lambda(0)$. We resolve this problem by using t-matrix calculations to estimate the scattering-dependent magnitude of the London penetration depth $\lambda(0, \Gamma)/\lambda(0, 0)$ and then use the well-known clean-limit value of $\lambda(0, 0) \approx 150$ nm from the previous measurements of high quality YBCO single crystals [7,31,34].

We note that the temperatures below $0.05T_c$ were excluded from the analysis due to a clear change in behavior. In YBCO, there are several possible complications at very low temperatures that lead to $1/T$-type behavior, such as Andreev bound states observed with our technique before [35] and/or effects of isolated impurities predicted for a d-wave superconductor [36]. However, thanks to high T_c, this is only a relatively small part in normalized units, $t = T/T_c$. Figure 2(a) shows the suppression of T_c as a function of irradiation dose, and Fig. 2(b) shows the best-fit exponent varying from $n = 1.15$ in the pristine state to $n = 1.8$ after second irradiation, clearly supporting the expected evolution from T-linear to T^2 behavior with the increase of the disorder scattering [11]. Since the decrease of T_c is a monotonic function of the scattering rate,

Γ, it can be used as the quantitative measure of the latter, thus eliminating the need to evaluate Γ explicitly.

The power-law fit is explored in Fig. 3 where the top panel (a) summarizes the exponent n obtained from the fit using different temperature intervals with the indicated upper limit for all three sample states considered here. This is done to explore how robust the exponent n is. Figure 3(b) shows the linear temperature dependence of the London penetration depth in a pristine state, behaving as expected for a clean d-wave superconductor with line nodes [2,4]. Interestingly, the linearity is extended up to quite high temperatures around 60 K (0.63 T_c). The abrupt change below 0.05 T_c is clearly not a smooth evolution and is likely where $1/T$ physics, unrelated to scattering, takes over. For the irradiated state, the situation is drastically different. Whereas the exponent, n, in the pristine state stays between 1.0 and 1.2, it increases from 1.4 to 1.7 for 6.15 C/cm^2 and from 1.7 to 1.9 for 8.5 C/cm^2 after irradiation. Notably, in the irradiated state, no good fix-exponent power-law fit was possible above 0.5 T_c and we observed a large variation of the power-law exponent at lower temperatures prompting us to explore a different fitting approach. The problem is that, as we will see from the numerical t-matrix analysis (Figs. 8 and 9 in the Appendix), weak scattering close to Born limit is not capable of turning T-linear behavior to quadratic, despite the fact that the transition temperature T_c is already substantially suppressed. In other words, T_c depends only on the scattering rate Γ, but Γ is a function of both impurity concentration and of the strength of the impurity scattering potential. For small strength, the suppression of T_c is achieved chiefly due to increasing concentration of scatterers. However, the T^2 behavior seems to be associated with the

FIG. 4. Lines show the exponent n obtained from the power-law fitting up to $T_c/3$, $\rho_s(t) = 1 - Rt^n$, of the superfluid density calculated numerically using the t-matrix theory. Different curves correspond to different values of the scattering potential strength, parameterized by the phase shift θ. The disorder is presented via the reduced $T_c(\Gamma)/T_{c0}$, also accessible experimentally. Symbols show the exponents obtained from the experiment, also fitted up to $T_c/3$. The best match is shown by a bold red line corresponding to $\theta = 70°$.
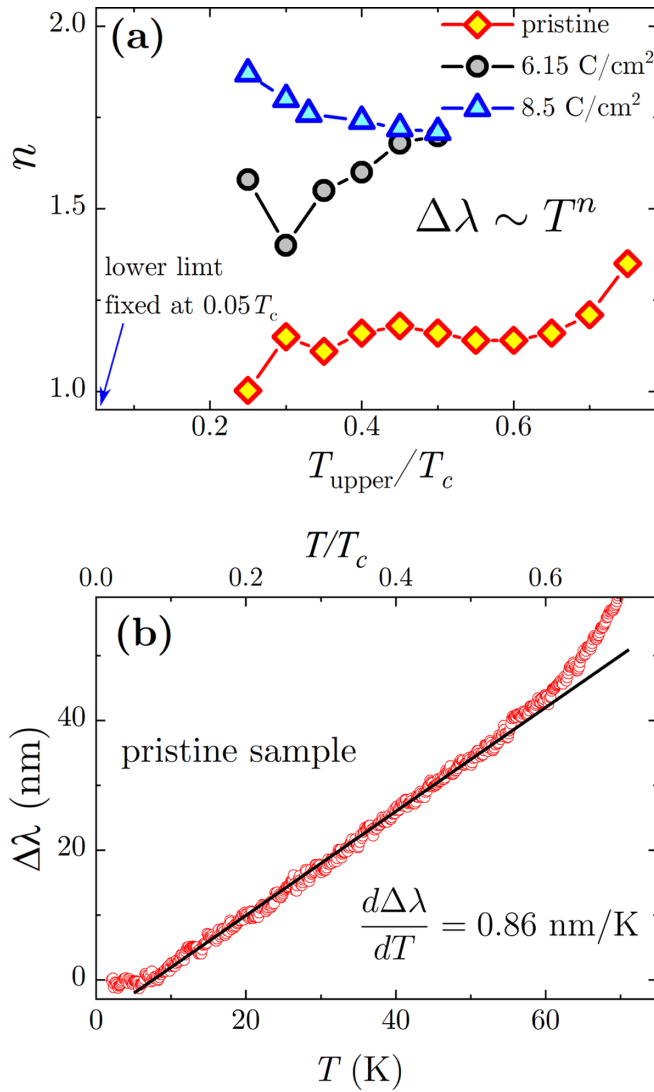
FIG. 3. (a) Results of a power-law fit, $\Delta\lambda \sim T^n$, as a function of the upper limit of the fitting range; see text for explanation. The lower limit was fixed at $T = 0.05\,T_c$. The exponent n jumps on irradiation from $n \approx 1$ in pristine state, toward $n = 2$ in the irradiated sample, inconsistent with the Born scattering limit. (b) London penetration depth in the pristine sample exhibiting an extended range of close to T-linear temperature dependence up to 60 K (about $0.63\,T_c$).

strong scattering potential, almost irrespective of the impurity concentration.

To analyze the obtained results and compare with the theory, we used t-matrix numerical analysis to calculate the superfluid density, $\rho_s(t, \Gamma)$. Details of the calculations are provided in Appendix A. The calculated $\rho_s(t, \Gamma)$ was fitted to the power law, fitting, $\rho_s(t) = 1 - Rt^n$; results are shown in Fig. 4. The fit was carried out up to $T_c/3$ for a particular fixed phase shift, θ, and fixed scattering rate, Γ, so that the large two-dimensional parameter space was covered. Each curve in Fig. 4 corresponds to a fixed θ and the x axis represents the scattering rate via the reduced suppression of the superconducting transition, $T_c(\Gamma)/T_{c0}(\Gamma = 0)$; see Fig. 7. The experimental data, also taken from the fitting up to $T_c/3$, are
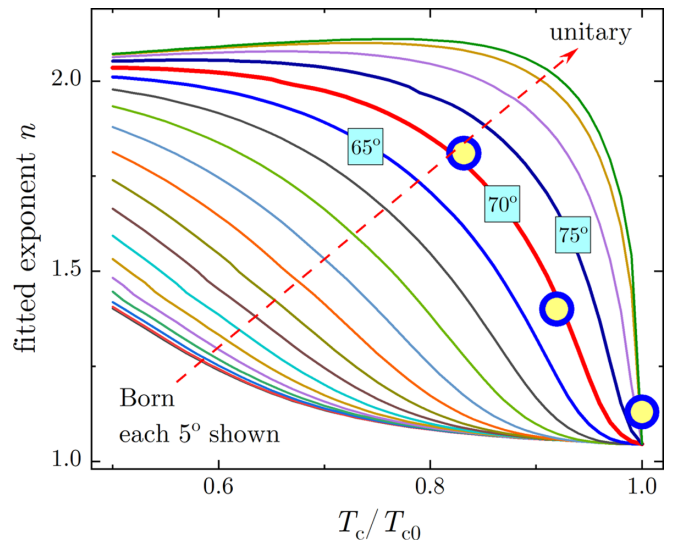
shown by symbols in Fig. 4. A good agreement is achieved with $\theta = 70°$ numerical curve.

To better understand the effect of scattering, we now analyze the linear to quadratic crossover by looking at the polynomial series representation, which allows comparing the coefficients (unlike the power law for which the prefactor has no particular meaning.)

Figure 5 shows results of the series polynomial expansion fit, $\rho_s \approx 1 - At - Bt^2$. The experimental data were fitted to match the same dimensionless coefficients to $2\Delta\lambda/\lambda(0, \Gamma) \approx At + Bt^2 \approx 1 - \rho_s$. The little problem here is that we do not know the value of $\lambda(0, \Gamma)$ after the irradiation. We therefore used $\lambda(0, 0) = 150$ nm of the pristine YBCO to calculate $\Delta\lambda/\lambda(0, 0)$ [7,31,34]. Now, multiplying both sides of the above equation by $\lambda(0, \Gamma)/\lambda(0, 0)$, we obtain $2\Delta\lambda/\lambda(0, \Gamma) \cdot \lambda(0, \Gamma)/\lambda(0, 0) = 2\Delta\lambda/\lambda(0, 0) \approx \tilde{A}t + \tilde{B}t^2$, where $[\tilde{A}, \tilde{B}] = [A, B] \cdot \lambda(0, \Gamma)/\lambda(0, 0)$. This way we only use experimental and/or calculated parameters but do not guess any numbers. Of course, this assumes that the calculated $\lambda(0, \Gamma)$ follows the model, but this is consistent since the same t-matrix model and parameters were used to calculate it. Figure 5 shows the renormalized coefficients $\tilde{A}$ and $\tilde{B}$ versus disorder scattering parameterized by T_c/T_{c0}. The same numerical $\rho_s(t, \Gamma/T_{c0})$ curves were used for the polynomial fitting as for the power-law analysis, Fig. 4.

Clearly, the quadratic term (the B coefficient) becomes progressively more dominant moving toward the unitary limit. However, we find that suggested in Ref. [11], the "interpolation formula" $\Delta\lambda/\lambda(0) = CT^2/(T^* + T)$ has a very narrow range of applicability. For example, by fitting the t-matrix numerical results we found that at $T_c/T_{c0} = 0.99$, the characteristic temperature is $T^* \approx 0.34T_c$ and at
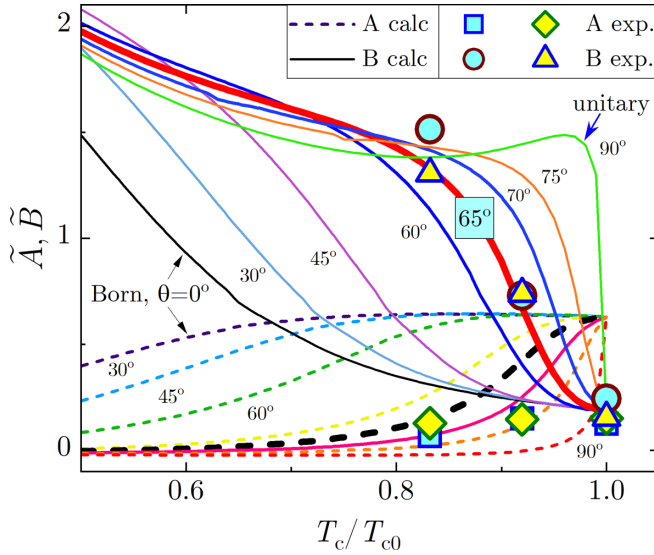
FIG. 5. Coefficients $\widetilde{A}$ and $\widetilde{B}$ obtained from the fitting of the t-matrix superfluid density to the quadratic polynomial $\rho_s = 1 - At - Bt^2$ and correcting for the change of the magnitude of $\lambda(0,0)$, namely, $[\widetilde{A}, \widetilde{B}] = [A, B] \cdot \lambda(0, \Gamma)/\lambda(0,0)$. This allows using only a known quantity, $\lambda(0,0) = 150$ nm, for the experimental $2\Delta\lambda/\lambda(0,0) \approx At + Bt^2 \approx 1 - \rho_s$. Dashed lines show $\widetilde{A}$ and solid lines show $\widetilde{B}$ coefficients, respectively. Different curves correspond to fixed values of the phase shift angle, θ, shown by the labels. The experimental data are shown by symbols, teal interior shows the upper limit of the polynomial fitting of $0.3T_c$, and yellow interior shows $0.4 T_c$ upper limit demonstrating the robust fit. The best match is shown by bold lines corresponding to $\theta = 65°$ phase shift in a close proximity to the value of $\theta = 70°$ obtained from the power-law fitting.

$T_c/T_{c0} = 0.98$, $T^* \approx 0.8 T_c$, both values already outside the "low-temperature" region of $0.3T_c$. For larger scattering, T^* practically diverges. Fitting the curves at a fixed $T_c/T_{c0} = 0.9$ for different θ reveals that T^* drops dramatically between $90°$ and $70°$ and then stays constant at about $T^* \approx 0.025T_c$. Therefore, while this approach was very useful for the discussion of the effect of disorder on a d-wave superconductor, we should not expect a quantitative agreement of the predicted temperature dependence with the experimental data.

By examining Fig. 5, we can formally assign the experimental data to $\theta = 65°$. These theoretical curves are shown by the thick lines. For the scattering phase shift of $65°$, we find the strength of the irradiation induced impurity potential about 70% of the inverse density of states. This is weaker than Schachinger and Carbotte's estimate [8]. In high-T_c cuprate superconductors, experimental studies of chemically substituted compounds determined that the inter-CuO_2-plane nonmagnetic disorder strength is closer to the unitary limit [37–39]. Further ion-specific studies are needed to elucidate this question. In the case of electron irradiation, electrons with energy tuned down to 0.7 MeV will mostly produce the in-plane disorder (see Appendix Fig. 10).

To understand our results, we analyze the effect of impurity scattering on the density of states, $N(\omega)$, for different values of the phase shift. Here $\hbar\omega$ is the quasiparticle energy measured from the Fermi energy. Transition temperature, T_c,
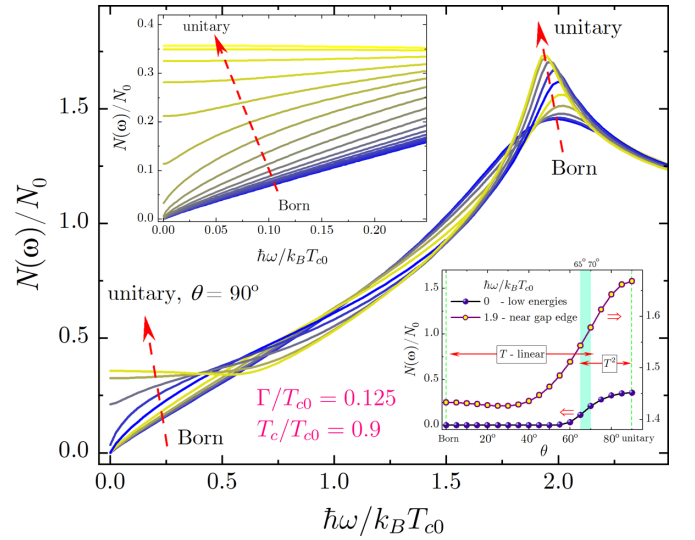

FIG. 6. The normalized density-of-states spectrum, $N(\omega)/N_0$, calculated by using a t-matrix theory for $\Gamma/T_{c0} = 0.125$ corresponding to $T_c/T_{c0} = 0.9$. The upper inset shows the low-energy region of $N(\omega)/N_0$. The curves are calculated in the interval $\theta = 0° - 90°$ with an equal increment of $\Delta\theta = 5°$. The apparent clustering of the curves for small $\theta \lesssim 45°$ is indicative of a weak scattering angle dependence of $N(\omega)$ in this interval. The lower inset shows the θ-dependent cuts taken at the Fermi level, at $\hbar\omega/k_B T_{c0} = 0$ (left axis) and near the gap edge, at $\hbar\omega/k_B T_{c0} = 1.9$ (right axis). Our experimental estimates of the phase shift between $\theta = 65°$ and $70°$ are shown by the green-shadowed rectangle. Interestingly that this is the range of a crossover from T-linear and T^2 behavior.

depends only on the scattering rate Γ, see Fig. 7, but Γ is a function of both impurity concentration and the strength of the impurity scattering potential. We used t-matrix analysis to compute $N(\omega)$ for a fixed $\Gamma/T_{c0} = 0.125$, which corresponds to $T_c/T_{c0} = 0.9$. Similar results would be obtained for any other fixed value. The normalized density of states is

$$\frac{N(\omega)}{N_0} = \text{Im}\left[\left\langle \frac{\tilde{\omega}}{\sqrt{\Delta_0^2 \cos^2(2\phi) - \tilde{\omega}^2}} \right\rangle_{FS}\right]. \quad (1)$$

Here $\langle...\rangle_{FS}$ denotes an average over the Fermi surface, N_0 is the normal metal density of states, and $\tilde{\omega}$ is the impurity renormalized energy; see Appendix A for details. The low-temperature behavior of the superfluid density, hence London penetration depth, is determined by the low-energy quasiparticle spectrum, $N(\omega \to 0)$. Strong and weak scatterers affect the functional form of $N(\omega)$ in very different ways. Weak scatterers are only able to break the pairs close to the gap edge, while strong scatterers produce resonant modes close to zero energy, thus significantly affecting low-temperature $\rho_s(t)$. Figure 6 shows the density-of-states spectrum in a full range of energies from zero to above the gap edge. Each curve is calculated for a fixed phase shift, from Born to unitary limit, in $10°$ steps. The upper inset zooms at the low-energy region showing curves for each $5°$. Clearly, low-energy $N(\omega)$ barely changes for small values of $\theta \lesssim 60°$ but then grows rapidly, and this induces the T^2 behavior. The way it happens is visualized in the lower inset in Fig. 6, where $N(\omega)/N(0)$ is plotted
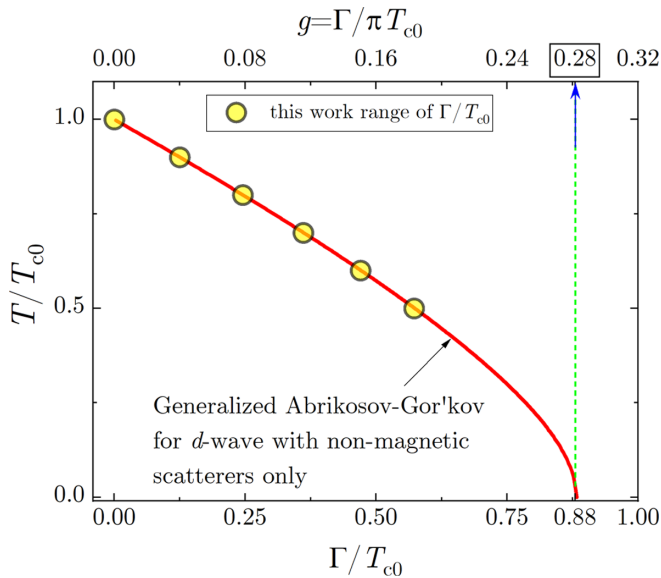
FIG. 7. Universal "Abrikosov-Gor'kov"-type dependence of the normalized superconducting transition temperature, T_c/T_{c0}, on the dimensionless scattering rate, Γ/T_{c0}. Bottom and top axes follow slightly different definitions used in the literature. The solid line shows the numerical solution of the Abrikosov-Gor'kov equation extended to arbitrary angular dependence of the order parameter, in this particular case to nonmagnetic impurities in a d-wave superconductor. Symbols show the range covered by the numerical t-matrix calculations presented in this paper.

for two fixed energies $\omega = 0$ (left y axis) and $\hbar\omega/k_B T_{c0} = 1.9$ (right y axis) at the peak region near the gap edge. Clearly the density of states does not change much until about $50°-60°$. Interestingly, this is the region consistent with our experiments. This re-enforces our conclusion that the observation of linear to quadratic crossover in the temperature dependence of $\rho(t)$ is a sensitive indicator of the scattering impurity strength.

We note that our estimates are based on a single-band d-wave model with only one in-band, scattering channel. However, in the case of YBa$_2$Cu$_3$O$_{7-\delta}$, there are two bands crossing the Fermi level centered around the **M** point [40–42]. The presence of multiple bands brings additional contribution of the interband impurity scattering; therefore the single-band estimate of the impurity potential strength is the upper bound. Experimental studies of multiband Ba$_{1-x}$K$_x$Fe$_2$As$_2$ [43] and BaFe$_2$(As$_{1-x}$P$_x$)$_2$ [44], where electron irradiation was used to introduce defects, support the intermediate strength of the scattering potential but not the unitary limit.

IV. CONCLUSIONS

Controlled point-like disorder induced by 2.5 MeV low-temperature electron irradiation was used to suppress superconductivity in a YBa$_2$Cu$_3$O$_{7-\delta}$ single crystal with the goal of determining the scattering potential strength in this high-T_c d-wave superconductor. The measured superconducting transition temperature, T_c, was used as the measure of the dimensionless scattering rate, Γ/T_{c0}. Normalized superfluid density was obtained from the measured London penetration depth, $\lambda(T)$, as well as from the t-matrix theory. By fit-

ting experimental and numerical data to two different models of the low-temperature behavior we estimated the scattering potential phase shift as approximately $\theta = 65°$ to $\theta = 70°$. These results find natural explanation when we consider how the density-of-states spectra, $N(\omega)$, are influenced by weak or strong scatterers. Only the latter affect the low-energy $N(\omega \rightarrow 0)$, which determines the low-temperature behavior of $\rho_s(t)$. Our results provide certain boundary conditions for the microscopic investigation of the pairing interactions and scattering in high-T_c cuprates for which the knowledge of the scattering phase shift is vital.

APPENDIX A: t-MATRIX APPROXIMATION FOR A SINGLE-BAND d-WAVE SUPERCONDUCTOR WITH NONMAGNETIC DISORDER SCATTERING

This Appendix provides some technical details of the t-matrix numerical analysis used in this paper.

The t-matrix approximation for the impurity scattering is based on the summation of all the single-site impurity scattering diagrams [45]; hence it is exact in the low impurity concentration limit. In general, the impurity dressed Green's function for a d-wave superconductor reads

$$\mathbf{G}(\mathbf{k}, i\omega_n) = -\frac{i\tilde{\omega}_n\tau_0 + \xi_{\mathbf{k}}\tau_3 + \Delta_{\mathbf{k}}\tau_1}{\tilde{\omega}_n^2 + \xi_{\mathbf{k}}^2 + \Delta_{\mathbf{k}}^2}, \quad \text{(A1)}$$

where $\xi_{\mathbf{k}}$ is the electronic dispersion, $\Delta_{\mathbf{k}}$ is the momentum superconducting gap, and ω_n is the fermionic Matsubara frequency. The impurity renormalized Matsubara frequency is denoted by $\tilde{\omega}_n$, which is

$$\tilde{\omega}_n = \omega_n + \frac{n_{\text{imp}}}{\pi N_0}\frac{g_0}{\cot^2\theta_s + g_0^2}, \quad \text{(A2)}$$

here n_{imp} is the impurity concentration, N_0 is the density of states at the Fermi energy, g_0 is

$$g_0 = \int_0^{2\pi}\frac{d\phi}{2\pi}\frac{\tilde{\omega}_n}{\sqrt{\tilde{\omega}_n^2 + \Delta_\phi^2}}, \quad \text{(A3)}$$

and θ_s is the s-wave scattering phase shift, defined as

$$\tan\theta_s = \pi N_0 V_{\text{imp}}. \quad \text{(A4)}$$

In the unitary limit, the s-wave scattering phase shift becomes $\pi/2$ as the impurity potential V_{imp} goes to ∞. Note we

assume an isotropic Fermi surface and restrict the momentum dependence of the gap to the Fermi surface ($\Delta_{\mathbf{k}} = \Delta_0 \cos 2\phi$); this is a reasonable approximation in the low-temperature limit.

The impurity dressed Green's function is used to calculate the gap,

$$\Delta_0 = 2\pi T V_d N_0 \sum_{\omega_n > 0}^{\Omega_c} \int_0^{2\pi} \frac{d\phi}{2\pi} \frac{\Delta_0 \cos^2 2\phi}{\sqrt{\tilde{\omega}_n^2 + \Delta_0^2 \cos^2 2\phi}}. \quad \text{(A5)}$$

Here we choose a simple separable pairing interaction $V_{\text{pair}} = V_d \cos 2\phi \cos 2\phi'$, and Ω_c is the pairing cutoff energy scale. A negative value of V_d means attractive interaction for d-wave superconductivity. The transition temperature is determined by

$$\log\left(\frac{T_c}{T_{c0}}\right) = \Psi\left(\frac{1}{2}\right) - \Psi\left(\frac{1}{2} + \frac{\Gamma}{2\pi T_c}\right), \quad \text{(A6)}$$

where T_{c0} is the clean limit T_c, Ψ is the digamma function, and Γ is the pair-breaking energy scale, which is the normal-state single-particle scattering rate and within the t-matrix approximation reads

$$\Gamma = \frac{n_{\text{imp}}}{\pi N_0} \frac{1}{\cot^2 \theta_s + 1}. \quad \text{(A7)}$$

Note for a single-band d-wave superconductor there is a universal energy scale that determines T_c suppression. In the Born limit, Γ is $n_{\text{imp}} \pi N_0 V_{\text{imp}}^2$. The variation of T_c as a function of this universal energy scale is shown in Fig. 7. The critical value of Γ sufficient to destroy superconductivity is $\pi \exp^{-\gamma} / 2T_{c0}$, where $\gamma \approx 0.577$ is the Euler-Mascheroni constant. Once we calculate the impurity dressed Green's function, we can calculate the normalized superfluid density, $\rho_s = n_s / n$,

$$\rho_s = 2\pi T \sum_{\omega_n > 0} \int_0^{2\pi} \frac{d\phi}{2\pi} \frac{\Delta_0^2 \cos^2 2\phi}{\left(\tilde{\omega}_n^2 + \Delta_0^2 \cos^2 2\phi\right)^{3/2}}, \quad \text{(A8)}$$

where n is the normal fluid density. The magnetic penetration depth can be expressed as $\lambda(T, \Gamma)/\lambda(0,0) = 1/\sqrt{\rho_s}$. Apart from magnetic penetration depth, another quantity of interest is the density of states [see Eq. (1)]. For the density of states, we perform the analytical continuation of the Matsubara frequency to the upper half the plane ($i\omega_n \rightarrow \omega + i0^+$) to obtain the renormalized energy ω. After analytic continuation, the equation for the renormalized energy reads

$$\tilde{\omega} = \omega + i0^+ + \frac{n_{\text{imp}}}{\pi N_0} \frac{g_\omega}{\cot^2 \theta_s - g_\omega^2}, \quad \text{(A9)}$$

where g_ω is

$$g_\omega = \int_0^{2\pi} \frac{d\phi}{2\pi} \frac{\tilde{\omega}}{\sqrt{\Delta_0^2 \cos^2 2\phi - \tilde{\omega}^2}}. \quad \text{(A10)}$$

Note $\tilde{\omega}$ is a complex quantity.

Figure 8 shows the suppression of the superfluid density at $T = 0$ by nonmagnetic impurities for (a) different strengths of the scattering potential varying between Born and unitary limits and (b) as a function of the measurable quantity, T_c/T_{c0}. Each curve corresponds to the fixed angle θ indicated in
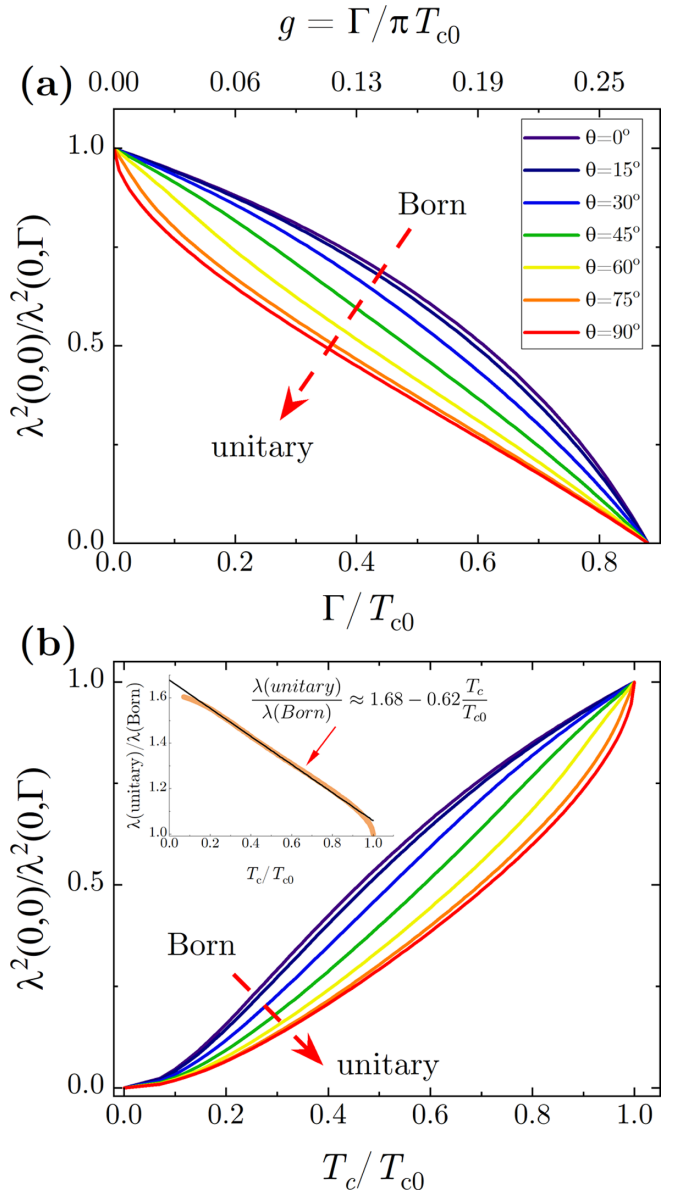

FIG. 8. Suppression of the superfluid density at $T = 0$ by nonmagnetic impurities for (a) different strengths of the scattering potential varying between Born and unitary limits and (b) as function of the measurable quantity, T_c/T_{c0}. Each curve corresponding to the fixed angle θ indicated in the legend. Panel (a) uses dimensionless scattering rates as top and bottom x axes. For a fixed scattering rate, London penetration depth, expectedly, increases the most in the unitary limit; however, it remains finite and the total change between two limits is less than a factor of two. This is shown in the inset in panel (b). A simple practical formula allowing estimation of the amplitude of the unitary limit is given, $\lambda(\text{unitary})/\lambda(\text{Born}) \approx 1.68 - 1.62(T_c/T_{c0})$.

the legend. Panel (a) uses two slightly different definitions of the dimensionless scattering rates as top and bottom x axes. For a fixed scattering rate, London penetration depth, expectedly, increases the most in the unitary limit; however, it remains finite and the ratio between the two limits is less than a factor of two. This is shown in the inset in panel (b). A simple practical formula allowing estimation of the amplitude of the unitary limit is given, $\lambda(\text{unitary})/\lambda(\text{Born}) \approx$
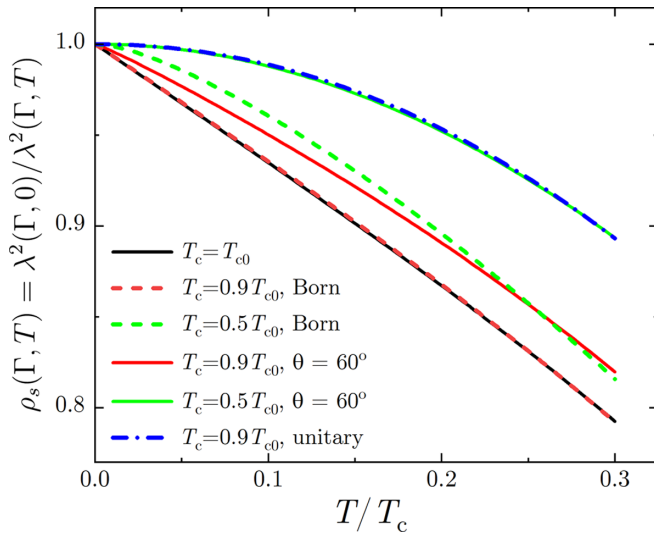
FIG. 9. Normalized superfluid density as a function of a reduced temperature in Born, unitary and intermediate scattering rate. For the same rate of T_c suppression, the curve is practically unchanged in the Born limit and shows quadratic behavior in unitary limit even for a moderate suppression.

$1.68 - 1.62(T_c/T_{c0})$. Note the variation of superfluid density is not universal like $T_c(\Gamma)$. This also reflects in the temperature dependence of the superfluid density in Fig. 9, where the unitary or stronger impurities bring the quadratic term very quickly for a very little T_c suppression.

APPENDIX B: ELECTRON IRRADIATION

Point-like disorder was introduced at the SIRIUS facility in the Laboratoire des Solides Irradiés at École Polytechnique in Palaiseau, France. Electrons accelerated in a pelletron-type accelerator to 2.5 MeV knock out ions creating vacancy-interstitial pairs (known as "Frenkel pairs") [25,26]. The acquired irradiation dose is determined by measuring the total charge accumulated by a Faraday cage located behind the sample. The sample is held in liquid hydrogen at around 20 K needed not only to remove significant amount of heat produced by subrelativistic electrons but also to prevent immediate recombination and migration of the produced atomic
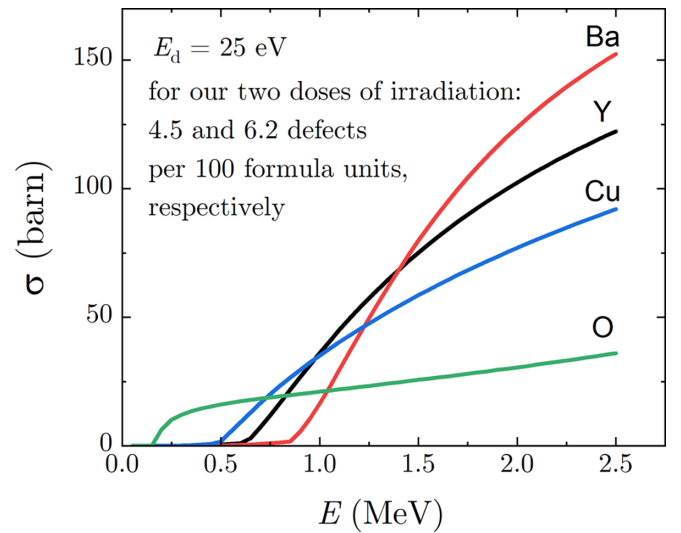

FIG. 10. Partial cross-section of atomic defects creation by electron irradiation of indicated energy. At our beam energy of 2.5 MeV the estimated total cross-section of any atom gives 4.5 and 6.2 defects per hundred formula units, assuming equal knock-out energy of 25 eV, typical for this kind of material [25,26]. The cross-sections are calculated using proprietary code SECTE developed at École Polytechnique specifically to describe electron irradiation experiments used in this paper.

defects. On warming to room temperature the interstitials that have lower barrier of diffusion migrate to various sinks (dislocations, twin boundaries, surfaces) faster, leaving the metastable population of vacancies. The achieved level of disorder induced by the irradiation is gauged by the change of resistivity. Detailed studies of YBCO samples from the same source are found elsewhere [18,19].

Ion-resolved cross-sections were calculated using SECTE software package developed at École Polytechnique specifically for the electron irradiation. Among different projectiles, electrons are best to produce point-like defects due to their small rest mass. As shown in Fig. 10, at our energy of 2.5 MeV, all YBCO ions are active and the estimated density of defects of any kind is about 5 defects per 100 formula units, which means that the defects are well separated and do not alter the material itself.

[1] J. G. Bednorz and K. A. Mueller, Z. Phys. B: Condens. Matter **64**, 189 (1986).

[2] D. Xu, S. K. Yip, and J. A. Sauls, Phys. Rev. B **51**, 16233 (1995).

[3] D. J. van Harlingen, Rev. Mod. Phys. **67**, 515 (1995).

[4] J. F. Annett, N. Goldenfeld, and A. J. Leggett, J. Low Temp. Phys. **105**, 473 (1996).

[5] K. M. Shen and J. C. S. Davis, Mater. Today **11**, 14 (2008).

[6] S.-L. Drechsler and T. Mishonov (eds.), *High-Tc Superconductors and Related Materials: Material Science, Fundamental Properties, and Some Future Electronic Applications*, 2001st ed., Nato Science Partnership Subseries: 3, 86 (Springer, Netherlands, 2001).

[7] W. N. Hardy, D. A. Bonn, D. C. Morgan, R. Liang, and K. Zhang, Phys. Rev. Lett. **70**, 3999 (1993).

[8] E. Schachinger and J. P. Carbotte, Phys. Rev. B **67**, 134509 (2003).

[9] P. W. Anderson, J. Phys. Chem. Solids **11**, 26 (1959).

[10] A. A. Abrikosov and L. P. Gor'kov, Zh. Eksp. Teor. Fiz. **39**, 1781 (1960) [Sov. Phys. JETP **12**, 1243 (1961)].

[11] P. J. Hirschfeld and N. Goldenfeld, Phys. Rev. B **48**, 4219 (1993).

[12] L. A. Openov, Phys. Rev. B **69**, 224516 (2004).

[13] L. A. Openov, J. Exp. Theor. Phys. Lett. **66**, 661 (1997).

[14] A. A. Golubov and I. I. Mazin, Phys. Rev. B **55**, 15146 (1997).

[15] V. G. Kogan, Phys. Rev. B **80**, 214532 (2009).

[16] D. V. Efremov, M. M. Korshunov, O. V. Dolgov, A. A. Golubov, and P. J. Hirschfeld, Phys. Rev. B **84**, 180512(R) (2011).

[17] J. Giapintzakis, D. M. Ginsberg, and M. A. Kirk, Technical Report (1995), doi:10.2172/510599.

[18] F. Rullier-Albenque, H. Alloul, and R. Tourbot, Phys. Rev. Lett. **91**, 047001 (2003).

[19] F. Rullier-Albenque, P. A. Vieillefond, H. Alloul, A. W. Tyler, P. Lejay, and J. F. Marucco, Europhys. Lett. **50**, 81 (2000).

[20] D. Achkir, M. Poirier, D. A. Bonn, R. Liang, and W. N. Hardy, Phys. Rev. B **48**, 13184 (1993).

[21] D. A. Bonn, S. Kamal, K. Zhang, R. Liang, D. J. Baar, E. Klein, and W. N. Hardy, Phys. Rev. B **50**, 4051 (1994).

[22] N. R. Lee-Hone, J. S. Dodge, and D. M. Broun, Phys. Rev. B **96**, 024501 (2017).

[23] R. Prozorov and V. G. Kogan, Rep. Prog. Phys. **74**, 124505 (2011).

[24] K. Cho, M. Kończykowski, S. Teknowijoyo, M. A. Tanatar, and R. Prozorov, Supercond. Sci. Technol. **31**, 064002 (2018).

[25] A. C. Damask and G. J. Dienes, *Point Defects in Metals* (Gordon & Breach Science Publishers Ltd, 1963).

[26] M. W. Thompson, *Defects and Radiation Damage in Metals*, revised September 27, 1974, ed., Cambridge Monographs on Physics (Cambridge University Press, 1969).

[27] R. Prozorov and R. W. Giannetta, Supercond. Sci. Technol. **19**, R41 (2006).

[28] D. L. Kaiser, F. Holtzberg, B. A. Scott, and T. R. McGuire, Appl. Phys. Lett. **51**, 1040 (1987).

[29] C. T. Van Degrift, Rev. Sci. Instrum. **46**, 599 (1975).

[30] R. Prozorov, R. W. Giannetta, A. Carrington, and F. M. Araujo-Moreira, Phys. Rev. B **62**, 115 (2000).

[31] R. Prozorov, R. W. Giannetta, A. Carrington, P. Fournier, R. L. Greene, P. Guptasarma, D. G. Hinks, and A. R. Banks, Appl. Phys. Lett. **77**, 4202 (2000).

[32] A. Carrington, C. R. Phys. **12**, 502 (2011).

[33] R. Prozorov, Phys. Rev. Appl. **16**, 024014 (2021).

[34] D. A. Bonn, R. Liang, T. M. Riseman, D. J. Baar, D. C. Morgan, K. Zhang, P. Dosanjh, T. L. Duty, A. MacFarlane, G. D. Morris, J. H. Brewer, W. N. Hardy, C. Kallin, and A. J. Berlinsky, Phys. Rev. B **47**, 11314 (1993).

[35] A. Carrington, F. Manzano, R. Prozorov, R. W. Giannetta, N. Kameda, and T. Tamegai, Phys. Rev. Lett. **86**, 1074 (2001).

[36] S.-W. Tsai and P. J. Hirschfeld, Phys. Rev. Lett. **89**, 147004 (2002).

[37] M. Salluzzo, F. Palomba, G. Pica, A. Andreone, I. Maggio-Aprile, O. Fischer, C. Cantoni, and D. P. Norton, Phys. Rev. Lett. **85**, 1116 (2000).

[38] M. Iavarone, M. Salluzzo, R. Di Capua, M. G. Maglione, R. Vaglio, G. Karapetrov, W. K. Kwok, and G. W. Crabtree, Phys. Rev. B **65**, 214506 (2002).

[39] H. Eisaki, N. Kaneko, D. L. Feng, A. Damascelli, P. K. Mang, K. M. Shen, Z.-X. Shen, and M. Greven, Phys. Rev. B **69**, 064512 (2004).

[40] S. V. Borisenko, A. A. Kordyuk, V. Zabolotnyy, J. Geck, D. Inosov, A. Koitzsch, J. Fink, M. Knupfer, B. Büchner, V. Hinkov, C. T. Lin, B. Keimer, T. Wolf, S. G. Chiuzbăian, L. Patthey, and R. Follath, Phys. Rev. Lett. **96**, 117004 (2006).

[41] V. B. Zabolotnyy, S. V. Borisenko, A. A. Kordyuk, J. Geck, D. S. Inosov, A. Koitzsch, J. Fink, M. Knupfer, B. Büchner, S.-L. Drechsler, H. Berger, A. Erb, M. Lambacher, L. Patthey, V. Hinkov, and B. Keimer, Phys. Rev. B **76**, 064519 (2007).

[42] T. Dahm, V. Hinkov, S. V. Borisenko, A. A. Kordyuk, V. B. Zabolotnyy, J. Fink, B. Büchner, D. J. Scalapino, W. Hanke, and B. Keimer, Nat. Phys. **5**, 217 (2009).

[43] K. Cho, M. Kończykowski, S. Teknowijoyo, M. A. Tanatar, Y. Liu, T. A. Lograsso, W. E. Straszheim, V. Mishra, S. Maiti, P. J. Hirschfeld, and R. Prozorov, Sci. Adv. **2**, e1600807 (2016).

[44] Y. Mizukami, M. Konczykowski, Y. Kawamoto, S. Kurata, S. Kasahara, K. Hashimoto, V. Mishra, A. Kreisel, Y. Wang, P. J. Hirschfeld, Y. Matsuda, and T. Shibauchi, Nat. Commun. **5**, 5657 (2014).

[45] P. J. Hirschfeld, P. Wölfle, and D. Einzel, Phys. Rev. B **37**, 83 (1988).